NIHON REOROJI GAKKAISHI Vol.27, No.2, 109〜115 (1999)


Article

# Measurement of Interfacial Tension between Polymer Melts: Improved Imbedded Fiber Retraction, Breaking Thread and Dynamic Viscoelasticity Methods

K. OKAMOTO[*1], M. TAKAHASHI[*1], H. YAMANE[*1], H. WATASHIBA[*1], Y. TSUKAHARA[*2], and T. MASUDA[*3]

[*1]*Department of Polymer Science and Engineering, Kyoto Institute of Technology, Sakyo-ku, Kyoto 606-8585, Japan*
[*2]*Department of Chemistry and Materials Technology, Kyoto Institute of Technology, Sakyo-ku, Kyoto 606-8585, Japan*
[*3]*Department of Material Chemistry, Kyoto University, Sakyo-ku, Kyoto 606-8501, Japan*
(Received: October 14, 1998)

We improved the imbedded fiber retraction (IFR) method as a simple method to obtain the interfacial tension between polymer melts. A force balance equation for a fiber in an immiscible matrix by Cohen and Carriere is solved for a more realistic fiber shape at later stage of retraction. Moreover, unknown hydrodynamic coefficient in the balance equation is determined theoretically as 0.125.

The interfacial tension between polystyrene (PS) and poly (methy methacrylate) (PMMA) is measured by the improved IFR (IIFR) method as well as the breaking thread method and dynamic viscoelasticity method. In dynamic viscoelasticity method, we determine the interfacial tension by fitting the Palierne theory with dynamic viscoelastic data. The interfacial tension obtained from the three methods agrees fairly well and is found to be about 1.6 mN $m^{-1}$ at 180°C and 1.4 mN $m^{-1}$ at 200°C.

**Key Words:** Interfacial tension / Polymer melts / Imbedded fiber retraction method / Breaking thread method / Dynamic viscoelasticity

## 1. Introduction

The interfacial tension is one of key factors which dominates morphology and viscoelastic properties of polymer blends.[1~4] The interfacial tension can be measured by various methods. These methods are divided into three classes. One is a class in which we use a balance equation between the interfacial tension and volumetric force acting on a droplet in a matrix polymer in steady state. The pendant drop method and spinning drop method belong to this class.[5~7] In this class, difference in density is essential to determine the interfacial tension at desired temperatures. Thus very accurate data of densities are necessary. In the second class, we observe the rate of shape change of interface. Two representative methods in this class are the imbedded fiber retraction (IFR) method[8] and the breaking thread (BT) method.[9] In this class, the zero shear viscosities of both polymers are necessary. As described in the subsequent section, a rheometer, a thermostat, a microscope, a camera, and a timer are enough to measure the interfacial tension. Therefore, these two methods are simple and useful to measure the interfacial tension. The third class is an indirect method to obtain the interfacial tension based on comparison[10] between dynamic viscoelastic data and the Palierne theory.[11] The Palierne theory predicts the dynamic viscoelasticity of polymer blends with island-sea structure from viscoelasticity of component polymers, interfacial tension, volume average droplet radius and volume fraction of droplets. In order to apply this method, we must observe morphology of the blend.

Cohen and Carriere analyzed the process of imbedded fiber retraction.[8] They approximated a shape of fiber to a cylinder with two hemispheres at both ends, and derived an equation which expresses the retraction process of the fiber. However, there are two problems in their analysis: (1) the modeled shape of droplet is different from the observed shape. (2) an unknown coefficient involved in their equation is evaluated by comparison with literature data.

Recently, Rundqvist et al. developed an imbedded disk retraction method.[12] They approximated the shape of a disk as an oblate spheroid. They observed that the shape of a disk changes into an oblate spheroid at early stage of shape recovery. Thus the first problem was solved. However, they also determined the unknown hydrodynamic coefficient by comparison with literature data. Luciani et al. measured the interfacial tension by using the recovery rate of small deformation of a droplet.[13] They only observed the shape change of a droplet corresponding to the last stage of the fiber retraction.

One of the objectives of the present study is to overcome the problems in the analysis of the IFR method. The other objective is to test applicability of the improved IFR (IIFR) method by comparing the interfacial tension obtained by this method with those by the BT and viscoelasticity methods.

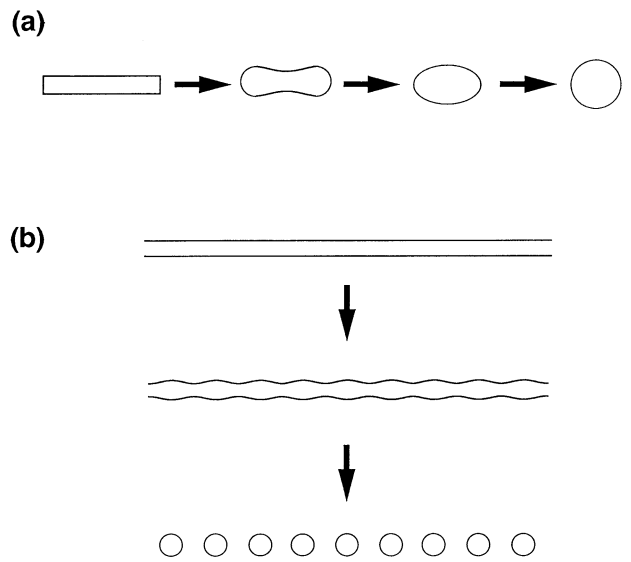


Fig.1 Change in the shape of fiber sample during measurements of the interfacial tension. The imbedded fiber retraction method (a) and the breaking thread method (b).

Fig.1 illustrates the shape change process of interface in the IIFR method (a) and the BT method (b). Fig.1(a) shows the time dependence of a short fiber in a matrix during the IIFR measurement. The shape of fiber changes into a dumbbell, an ellipsoid of revolution, and finally to a sphere. We observe this process by a microscope. Then the interfacial tension is calculated from the rate of fiber retraction in the state of ellipsoid of revolution. Fig.1(b) illustrates the time evolution of the shape of a thread like fiber in the BT method. In this process, the distortion on interface of the thread grows with time, and the thread breaks into spheres. We determine the interfacial tension from the growth rate of distortion.

## 2. Theory

### 2.1 Improved Imbedded Fiber Retraction Method

Cohen and Carriere[8] obtained a differential equation for a force balance between the interfacial tension and viscous resistance.

$$\alpha \frac{\mathrm{d}A}{\mathrm{d}L} + 6\pi\chi\eta_e R \frac{\mathrm{d}L}{\mathrm{d}t} = 0 \qquad (1)$$

In this equation, $\alpha$, $\chi$ and $\eta_e$ denote the interfacial tension, the unknown hydrodynamic coefficient and the effective viscosity, respectively. The shape of fiber is expressed through *A*, *L* and *R* which are the interfacial area, overall length of cylinder with hemispherical ends, and the radius of cylinder, respectively.

We approximate the shape of fiber as an ellipsoid of revolution at the later stage of retraction based on experimental observation shown later. Then, *A*, *L*, and *R* can be substituted respectively by normalized interfacial area $\hat{A}$ twice of normalized semimajor axis $2\hat{a}$, and normalized semiminor axis $\hat{b}$ of the ellipsoid of revolution. Here, normalized axes and interfacial area are defined as

$$\hat{a} = \frac{a}{r_0},\ \hat{b} = \frac{b}{r_0},\ \text{and}\ \hat{A} = \frac{A_{ER}}{4\pi {r_0}^2} \qquad (2)$$

where $r_0$ denotes the radius of droplet with spherical shape at equilibrium state, and $A_{ER}$ is the interfacial area of the ellipsoid of revolution with major axis 2a and minor axes 2b and 2c (= 2b). Using these normalized quantities, the balance equation is expressed as

$$\alpha \frac{\mathrm{d}\hat{A}}{\mathrm{d}\hat{a}} + 6\chi r_0 \eta_e \hat{b} \frac{\mathrm{d}\hat{a}}{\mathrm{d}t} = 0 \qquad (3)$$

The normalized surface area $\hat{A}$ of an ellipsoid of revolution is given by

$$\hat{A} = \frac{1}{2}\left[\hat{b}^2 + \frac{\arcsin\sqrt{1-\hat{b}^6}}{\sqrt{1-\hat{b}^6}}\frac{1}{\hat{b}}\right] \qquad (4)$$

In eq.(4), we used the assumption of volume conservation given by

$$\hat{a}\hat{b}^2 = 1 \qquad (5)$$

To solve eq. (3) analytically, we approximate $\hat{A}$ by the following form.

$$\hat{A} = \frac{1}{2}\left(\hat{b}^2 - 1 + \frac{2}{\hat{b}}\right) \qquad (6)$$

Fig.2 compares the normalized area with approximated normalized area. The relative error due to this approximation is less than 0.002 at $\hat{b} \geq 0.7$.

From eqs. (3), (5) and (6), we get the following equation.

$$\int \frac{\mathrm{d}\hat{b}}{\hat{b}^3 - \hat{b}^6} = \int \frac{\alpha}{24\chi r_0 \eta_e}\,\mathrm{d}t \qquad (7)$$

This equation is solved analytically, and the solution is

$$f\left(\hat{b}\right) - f\left(\hat{b}_0\right) = \frac{\alpha}{24\chi r_0 \eta_e}(t - t_0) \qquad (8)$$

where $f\left(\hat{b}\right)$ is given by the following equation.

$$f\left(\hat{b}\right) = -\frac{1}{2\hat{b}^2} - \frac{1}{6}\ln\left[\frac{\left(\hat{b}-1\right)^2}{\hat{b}^2+\hat{b}+1}\right] + \frac{1}{\sqrt{3}}\arctan\left[\frac{2\hat{b}+1}{\sqrt{3}}\right] \qquad (9)$$

In eq.(8), $\hat{b}_0$ represents $\hat{b}$ at $t = t_0$, where $t_0$ is the time when the shape of the droplet becomes an ellipsoid of revolution. We cannot determine $t_0$ exactly but can evaluate the interfacial

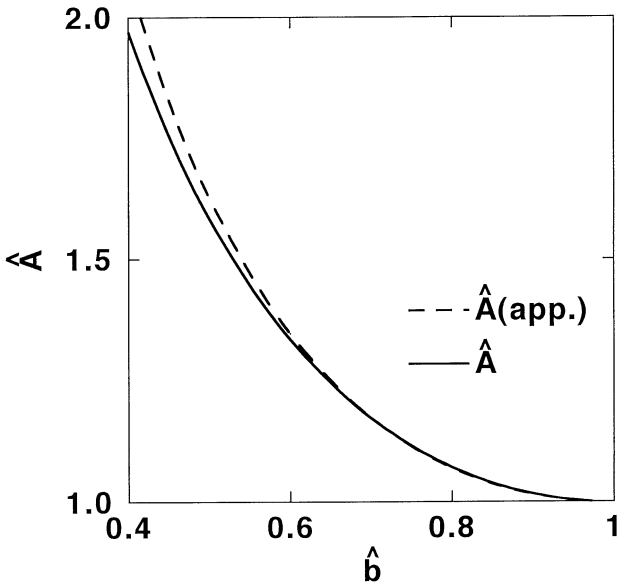


Fig.2 Exact and approximated normalized surface areas plotted against normalized semiminor axis.

tension using eq.(8) from the slope of a plot of $f(\hat{b})$ against t. However, eq.(8) contains the unknown coefficient $\chi$ and the unknown effective viscosity $\eta_e$. For $\eta_e$ we adopt Rallison's expression.[14]

$$\eta_e = \eta_m \frac{(19K+16)(2K+3)}{40(K+1)} \tag{10}$$

Here $\eta_m$ represents the viscosity of the matrix. The viscosity ratio $K$ in eq.(10) is defined as $K = \eta_d/\eta_m$ where $\eta_d$ denotes the viscosity of the droplet.

At long times, $\hat{b}$ approaches unity and $f(\hat{b})$ is approximated to be

$$f(\hat{b}) \cong -\frac{1}{3}\ln(1-\hat{b}) - \frac{1}{2} + \frac{1}{6}\ln 3 + \frac{\pi}{3\sqrt{3}} \tag{11}$$

From eqs.(8) and (11), $\hat{b}$ becomes a simple function of $t$ as

$$\hat{b} = 1 - C\exp\left[-\frac{3t}{\tau_{ER}}\right] \tag{12}$$

where

$$\tau_{ER} = \frac{24\chi r_0 \eta_e}{\alpha} \tag{13}$$

$$C = \exp\left[3\left(-\frac{1}{2} + \frac{1}{6}\ln 3 + \frac{\pi}{3\sqrt{3}} - f(\hat{b}_0) + \frac{t_0}{\tau_{ER}}\right)\right] \tag{14}$$

From eqs.(5) and (12), we get

$$\ln \hat{a} = -2\ln\left[1 - C\exp\left[-\frac{3t}{\tau_{ER}}\right]\right] \cong 2C\exp\left[-\frac{3t}{\tau_{ER}}\right] \tag{15}$$

This equation indicates that $\ln(a/r_0)$ decreases with $t$ exponentially at long time end of retraction and the retraction time is given by $\tau_{ER}/3$. This behavior agrees with the results obtained in our previous paper.[15] In our previous paper, we found that $\ln(a/r_0)$ of a single droplet after application of step shear strain decreases exponentially at long time end of shape recovery. The recovery time is found to be equal to the linear viscoelastic relaxation time of the droplet, $\tau_D$, given by the Palierne theory[3), 11)] as

$$\tau_D = \frac{r_0\eta_m}{\alpha}\frac{(19K+16)(2K+3)}{40(K+1)} \tag{16}$$

Here the volume fraction of the droplet is extrapolated to be zero. This behavior agrees with prediction of Rallison[14] for a small deformation of a single droplet.[13] Equating $\tau_{ER}/3$ with $\tau_D$, we obtain $\chi$ as 0.125. We then get the interfacial tension by using eq.(8) with the values of $\eta_m$, $\eta_d$ and $r_0$.

### 2.2 Breaking Thread Method

In this method we observe distortion on the interface of a polymer thread imbedded in a polymer matrix. This distortion is called as the Rayleigh wave. Elemans et al. determined the interfacial tension by observing the time evolution of the distortion and using the Tomotika theory.[9), 16)]

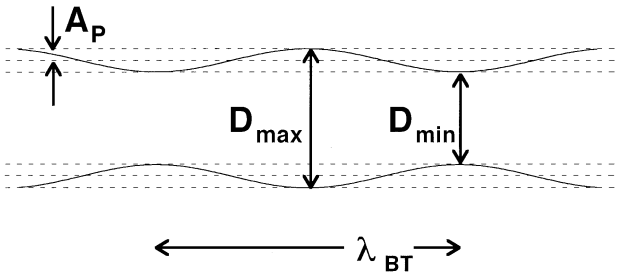


Fig.3 Distortion on the interface between a thread and a matrix.

In the BT method, the distortion is approximated to be sine wave as illustrated in Fig.3. In this figure, $A_p$, $\lambda_{BT}$, $D_{max}$ and $D_{min}$ denote the amplitude of distortion, the wave length of distortion, the maximum diameter of the thread and the minimum diameter of the thread, respectively. Tomotika predicted time evolution of the amplitude as

$$A_p = A_0 \exp[q(t - t_0)] \quad (17)$$

where $t$, $A_0$ and $q$ denote the time, the amplitude at $t = t_0$ and the growth rate of the distortion, respectively. The time $t_0$ is taken as the time when original amplitude arises. The growth rate $q$ is expressed as

$$q = \frac{\alpha\Omega(\lambda_{BT}, K)}{\eta_m D_0} \quad (18)$$

where $D_0$ denotes the initial thread diameter and $\Omega$ ($\lambda_{BT}$, $K$) represents the Tomotika function given by Eqs.(38)-(40) in reference 16 as a function of $\lambda_{BT}$ and $K$. We evaluate the growth rate $q$ experimentally by using eq.(17). The rate $q$ is determined from the plot of $\log(2A_p/D_0)$ against $t$. The interfacial tension $\alpha$ is calculated from eq.(18).

## 3. Experimental

### 3.1 Materials

Two pairs of polystyrene (PS) and poly (methyl methacrylate) (PMMA) are used in this study. One pair consists of two samples with narrow molecular weight distribution Polystyrene F20 (TOYO SODA Co., Ltd.) and Poly(methyl methacrylate) MF9. The sample MF9 was synthesized by anionic polymerization as described in reference 17. Another pair contains two samples with broad molecular weight distribution PS679 (Asahi Chemical Co., Ltd.) and PMMA037A (Scientific Polymer Products).

Table I summarizes the average molecular weights and their ratio of samples before and after measurements of the interfacial tension. The weight-average and number-average molecular weights, Mw and Mn, and the ratio Mw/Mn were determined by gel permeation chromatography (TOYO SODA HLC-802A). We do not see any indication of degradation during the measurements of the interfacial tension in Table I.

Table I Average molecular weights and their ratio of component polymers before and after measurements of the interfacial tension.

| sample | temperature /°C | $M_w/10^4$ | $M_n/10^4$ | $M_w/M_n$ |
|---|---|---|---|---|
| F20 before | - | 17.6 | 16.1 | 1.10 |
| after | 200 | 18.4 | 16.6 | 1.11 |
| after | 180 | 18.5 | 16.5 | 1.12 |
| MF9 before | - | 5.14 | 4.40 | 1.17 |
| after | 200 | 5.25 | 4.50 | 1.17 |
| after | 180 | 5.17 | 4.46 | 1.16 |
| PS679 before | - | 18.7 | 9.27 | 2.02 |
| after | 200 | 18.2 | 9.08 | 2.01 |
| PMMA037A before | - | 3.43 | 2.10 | 1.63 |
| after | 200 | 3.48 | 2.10 | 1.66 |

### 3.2 Sample preparation

Matrix polymers were melt-pressed into disks with 30 mm diameter and 2-3 mm thickness for the IIFR and BT methods. Temperatures for the melt press were 170°C for F20 and 185°C for PS679 and PMMA037A, respectively. The fibers of PS679 and PMMA037A were melt spun by use of a capillary rheometer (TOYO SEIKI CAPIROGRAPH) at 190°C. The fiber of MF9 was made by elongation on a hot plate at 180°C. The diameter of these fibers is 20-30 μm. The fibers with the length about 2 mm for the IIFR method and 10-15 mm for the BT method were placed between two plates of matrix and the fibers were imbedded in the plates by heat treatment. The pair of MF9 fiber/ F20 matrix was adhered by heating at 150°C in the same isothermal bath as that used in measurements for 20 minutes in nitrogen flow of 10 l/min. The pairs of PS679 fiber / PMMA037A matrix and PMMA037A fiber / PS679 matrix were melt-pressed at 160°C and 145°C, respectively. In the BT experiment, the aspect ratio of the fiber should be more than 60 to avoid end pinching.[9] In order to eliminate the effect of boundary between matrix and outer space, thickness of matrix should be at least 10 times lager than the diameter of the fiber.

For the dynamic viscoelasticity measurement, samples were pressed into disks with 24 mm diameter and 1.2-1.5 mm thickness by melt press at 160°C. All the samples for the IIFR, BT and viscoelasticity methods were dried in a vacuum oven at 80°C for more than 4 hours before each heat treatment and measurement.

### 3.3 IIFR and BT methods

The sample in a glass cell was placed in an isothermal bath. The isothermal bath was thermostated at required temperature, and the nitrogen flowed in the bath with the rate of 10 l/min. We observed the shape of the fiber by use of a stereo microscope through a window of the bath, and recorded the shape change by taking pictures with time. It is noteworthy that the shape change of interface occurs much slower than relaxation of polymer chains. Therefore, molecular orientation of spun fiber does not affect the rate of shape change.

In order to obtain radius of final spherical droplet, it was confirmed that semimajor axis $a$ does not change more than an hour at the end of the IIFR measurement.

### 3.4 Rheological measurement

Dynamic viscoelasticity measurement was carried out using Rheometrics RDA-II and Bohlin CSM with 25 mm$\phi$ parallel plate geometries. The zero shear viscosities $\eta_0$ of PS and PMMA were determined from frequency dependencies of the loss modulus $G''$ at low frequency limit.

## 4. Results and Discussion

Table II summarizes the zero shear viscosity of each polymer at indicated temperatures obtained from the dynamic viscoelasticity measurement.

Table II The zero shear viscosity of component polymers.

| sample | code | temperature/°C | $\eta_0$/Pa s |
|---|---|---|---|
| PMMA | MF9 | 180 | $9.01\times10^4$ |
| | | 200 | $1.04\times10^4$ |
| PS | F20 | 180 | $3.93\times10^4$ |
| | | 200 | $8.03\times10^3$ |
| PMMA | 037A | 200 | $3.55\times10^3$ |
| PS | 679 | 200 | $2.99\times10^3$ |

Fig.4 shows micrographs during retraction of a MF9 short fiber imbedded in a F20 matrix. At middle stage, the shape of fiber is dumbbell like as shown in Figs. 4 (a) and (b). In the course of retraction process, the shape of fiber becomes an ellipsoid of revolution as shown in Fig. 4 (c), then the fiber retracts as illustrated in Fig. 4 (d) and (e). Finally, the droplet attains a spherical shape as shown in Fig. 4 (f). Similar results are obtained for other samples with different viscosity ratios.

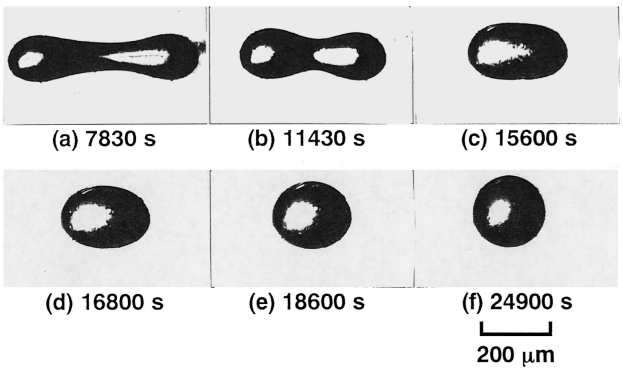


Fig.4 Micrographs of retraction for a MF9 short fiber imbedded in a F20 matrix at 200 °C: (a) t = 7830 s, (b) 11430 s, (c) 15600 s, (d) 16800 s, (e) 18600 s, (f) 24900 s.

Fig.5 shows time dependence of $f\left(\hat{b}\right)$ for a MF9 fiber in a F20 matrix at 200°C. The normalized length is calculated from the observed lengths $a$ and $r_0$ by use of eq.(5). Fig.5 indicates that the prediction of eq.(8) agrees with the experimental result. We evaluate the interfacial tension from the slope of the solid line in Fig.5. The value of $\alpha$ is summarized in Table III. The value of experimentally obtained $f\left(\hat{b}\right)$ contains an error caused by an error of $\hat{a}$. The error of $f\left(\hat{b}\right)$ is estimated as

$$\left|\frac{\Delta f\left(\hat{b}\right)}{f\left(\hat{b}\right)}\right| = \left|\frac{\frac{\partial f}{\partial \hat{b}}\frac{\partial \hat{b}}{\partial \hat{a}}\Delta\hat{a}}{f\left(\hat{b}\right)}\right| = \left|\frac{1}{2}\frac{\hat{a}^{\frac{5}{2}}}{\hat{a}^{\frac{3}{2}}-1}\frac{1}{f\left(\hat{b}\right)}\right|\left|\frac{\Delta\hat{a}}{\hat{a}}\right| \quad (19)$$

The error in measurement of $\hat{a}$, $\Delta\hat{a}/\hat{a}$, was 1.5%. The error bars in Fig.5 are evaluated by eq.(19).

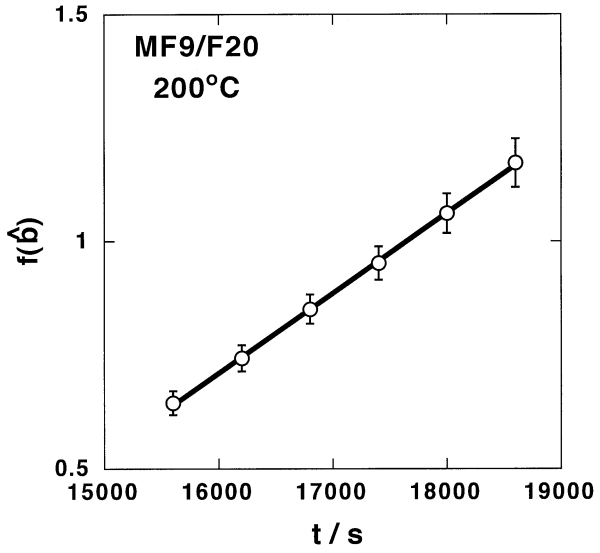


Fig.5 Plot of $f\left(\hat{b}\right)$ against time for a MF9 fiber in a F20 matrix at 200°C.

Fig.6 gives micrographs showing the growth of distortion for a PS679 fiber imbedded in a PMMA037A matrix. The shape of interface can be approximated by sine wave in Fig.6 (b) - (e). However the shape deviates from sine wave at later stage of the measurement shown in Fig.6 (f). We determine the interfacial tension from Fig.6 (b)-(e) where the shape of interface is represented by sine wave .

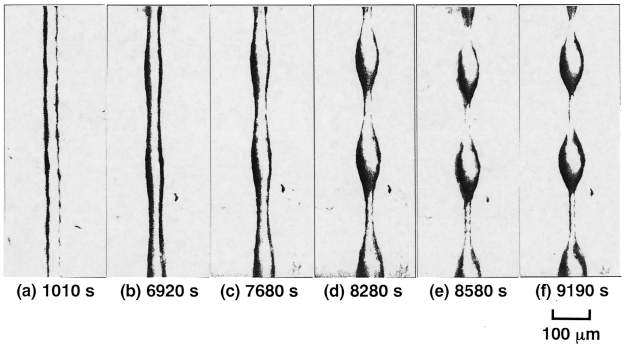


Fig.6 Micrographs showing the growth of distortion for a PS679 fiber in a PMMA037A matrix at 200 °C: (a) t = 1010 s, (b) 6920 s, (c) 7680 s, (d) 8280 s, (e) 8580 s, (f) 9190 s.

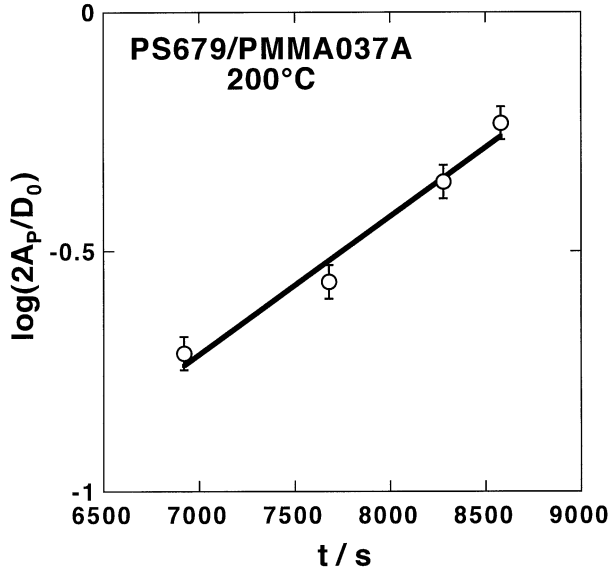


Fig.7 Plot of $\log(2A_p/D_0)$ against time for a PS679 fiber in a PMMA037A matrix at 200°C.

Fig.7 shows the time dependence of $\log(2A_p/D_0)$ for a PS679 fiber in a PMMA037A matrix. The amplitude of distortion, $A_p$, is given by

$$A_p = \frac{D_{max} - D_{min}}{4} \tag{20}$$

The data of $\log(2A_p/D_0)$ is a linear function of the time $t$. This behavior agrees with the prediction of eq.(17). From the slope of the plot of $\log(2A_p/D_0)$ against $t$, we get the growth rate $q$. We then evaluate the interfacial tension from eq.(18) using the calculated value of $\Omega$ ($\lambda_{BT}$, $K$). The error bars in Fig.7 are calculated using the following equation.

$$\left|\frac{\Delta \log\left(\frac{2A_p}{D_0}\right)}{\log\left(\frac{2A_p}{D_0}\right)}\right| = \left|\frac{1}{2.303\log\left(\frac{2A_p}{D_0}\right)}\right| \left|\frac{\Delta\left(\frac{2A_p}{D_0}\right)}{\left(\frac{2A_p}{D_0}\right)}\right| \tag{21}$$

The error in measuring $2A_p/D_0$ was 8% in our experiment.

Fig.8 shows dynamic moduli for a sample of F20/MF9 = 20/80 blend at 200°C. Solid and dashed lines indicate the best fit by the Palierne theory.[11] For calculation of the fitting curves, we use the dynamic moduli of the component polymers and the volume average radius of droplets. The interfacial tension is treated as a parameter. Details of evaluation of the interfacial tension by dynamic viscoelasticity was described in the reference 10.

Table III summarizes the interfacial tension obtained by the three methods for the two pairs of PS/PMMA samples. The experimental error in the interfacial tension is estimated using the error of $f(\hat{b})$ for the IIFR method and $\log(2A_p/D_0)$ for the BT method. As to the dynamic viscoelasiticity method, the

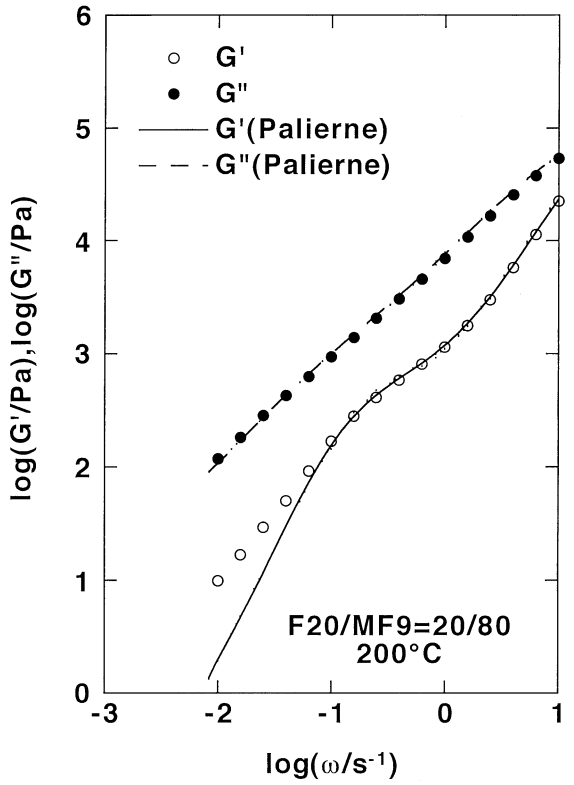


Fig.8 Dynamic moduli for a sample of F20/MF9 = 20/80 blend at 200°C. Solid and dashed lines represent the best fit of calculated moduli by the Palierne theory.

Table III The interfacial tension measured by the IIFR, BT, and dynamic viscoelasticity methods.

| fiber sample | matrix sample | temperature /℃ | α/mN m$^{-1}$ (IIFR) | α/mN m$^{-1}$ (BT) | α/mN m$^{-1}$ (dynamic viscoelasticity) |
|---|---|---|---|---|---|
| MF9 | F20 | 180 | 1.6±0.2 | - | 2.3±0.4 |
| MF9 | F20 | 200 | 1.4±0.2 | - | 1.65±0.35 |
| PS679 | PMMA037A | 200 | 1.4±0.2 | 1.1±0.2 | - |
| PMMA037A | PS679 | 200 | - | 1.5±0.4 | - |

error amount to about 20%, which is due to the sample preparation, the measurement of the dynamic moduli and the fitting with the theory. By the fitting with the Palierne theory, upper and lower values of $\alpha$ are evaluated. The interfacial tension tabulated in Table III is mean value of these limit values and deviation from these values for dynamic viscoelasticity method. From the value of the interfacial tension between PS679 and PMMA037A determined by the BT method, it seems that exchange of fiber and matrix affects somewhat measured values. Comparing $\alpha$ for PS679/PMMA037A obtained by the BT method with that obtained by the IIFR method, we find that measured $\alpha$ is similar in both methods. This experimental result indicates that eq.(8) and evaluated α value are appropriate. Next we compare α for MF9/F20 samples obtained by the IIFR method with that

obtained by the dynamic viscoelasticity method. The interfacial tension $\alpha$ measured by both methods agrees fairly well at 200°C.

Comparing the three measurement methods, some good and weak points of each method become clear. In the IIFR method, semimajor axis a is parallel to the fiber axis. On the other hand, amplitude of distortion is perpendicular to the fiber axis in the breaking thread method. The length measured in the IIFR method is longer than that in the BT method. Thus, the error inherent in measuring the length is smaller in the IIFR method than that in the BT method, using the fiber with the same diameter and the same apparatus. As a result of this error, the error in the determined interfacial tension is smaller for the IIFR method. It is possible to make the error in measuring the amplitude smaller by using a fiber with larger diameter in the BT method. However, it takes longer time for measurement of the thicker fiber. The longer experimental time causes the higher degradation of sample. In addition, a large amount of sample is necessary for the measurement using the thick fiber. For these reasons, the IIFR method is more adequate than the BT method for the experiment using a simple apparatus and a small amount of sample. As to the dynamic viscoelasticity method, it is necessary to make blends and observe morphology of the blends to determine the interfacial tension. Thus, this method is not simple for evaluation of the interfacial tension.

## 5. Conclusions

We improved the IFR method by approximating the droplet shape as an ellipsoid of revolution. The derived equation using this approximation agrees with experimental results for PS/PMMA. Moreover, we theoretically calculated the unknown hydrodynamic coefficient $\chi$. The coefficient $\chi$ is estimated to be 0.125.

We measured the interfacial tension of PS/PMMA by use of the improved IFR method, BT method, and dynamic viscoelasticity method. The interfacial tension given by these methods agrees fairly well with each other: $\alpha$ is about 1.6 mN $m^{-1}$ at 180°C and 1.4 mN $m^{-1}$ at 200°C.

The IIFR method is the simplest and the most definite method in the three methods investigated in the present paper. It is possible in the IIFR method to measure definite length of desired position on the shape of interface using the simple apparatus.

## References


1) Grace HP, *Chem Eng Commun*, **14**, 225 (1982).
2) Wu S, *Polym Eng Sci*, **27**, 335 (1987).
3) Graebling D, Muller R, Palierne JF, *Macromolecules*, **26**, 320 (1993).
4) Maeda S, Kamei E, *Nihon Reoroji Gakkaishi*, **22**, 145 (1994).
5) Anastasiadis SH, Gancarz I, Koberstein JT, *Macromolecules*, **21**, 2980 (1988).
6) Fukunaga K, Maeda S, Kamei E, *Kobunshi Ronbunshu*, **53**, 352 (1996).
7) Joseph DD, Arney MS, Gillberg G, Hu H, Hultman D, Verdier C, Vinagre TM, *J Rheol*, **36**, 621 (1992).
8) Cohen A, Carriere CJ, *Rheol Acta*, **28**, 223, (1989).
9) Elemans PHM, Janssen JMH, Meijer HEH, *J Rheol*, **34**, 1311 (1990).
10) Okamoto K, Takahashi M, Yamane H, Kashihara H, Masuda T, *Nihon Reoroji Gakkaishi*, **25**, 199 (1997).
11) Palierne JF, *Rheol Acta*, **29**, 204 (1990).
12) Rundqvist T, Cohen A, Klason C, *Rheol Acta*, **35**, 458 (1996).
13) Luciani A, Champagne MF, Utracki LA, *J Polym Sci B: Polym Phys*, **35**, 1393 (1997).
14) Rallison JM, *Ann Rev Fluid Mech*, **16**, 45 (1984).
15) Yamane H, Takahashi M, Hayashi R, Okamoto K, Kashihara H, Masuda T, *J Rheol*, **42**, 567 (1998).
16) Tomotika S, *Proc Roy Soc London Ser A*, **150**, 322 (1935).
17) Masuda T, Kitagawa K, Onogi S, *Polymer J*, **1**, 418 (1970).